Comparison of electrochemical hydrogen oxidation on different metal/ceramic model anodes and mechanistic implications

JPhys Energy

OPEN ACCESS

RECEIVED
20 February 2019

REVISED
14 April 2019

ACCEPTED FOR PUBLICATION
2 May 2019

PUBLISHED
25 July 2019

PAPER

Comparison of electrochemical hydrogen oxidation on different metal/ceramic model anodes and mechanistic implications

M C Doppler[1,2], **J Fleig**[2], **M Bram**[1,3] and **A K Opitz**[1,2,4]

[1] Christian Doppler Laboratory for Interfaces in Metal-Supported Electrochemical Energy Converters, Forschungszentrum Jülich, Wilhelm-Johnen-Straße, D-52425 Jülich, Germany
[2] Institute of Chemical Technologies and Analytics, TU Wien, Getreidemarkt 9-164/EC, A-1060 Vienna, Austria
[3] Institute of Energy Research (IEK-1), Forschungszentrum Jülich, Wilhelm-Johnen-Straße, D-52425 Jülich, Germany
[4] Author to whom any correspondence should be addressed.

E-mail: michael.doppler@tuwien.ac.at, j.fleig@tuwien.ac.at, m.bram@fz-juelich.de and alexander.opitz@tuwien.ac.at

Keywords: pattern anodes, impedance spectroscopy, hydrogen oxidation mechanism, SOFC/SOEC

Abstract

Micro-patterned metal/ceramic model thin film electrodes were used to investigate the hydrogen oxidation mechanism on various metal/ion conductor combinations such as Ni/yttria-stabilized zirconia (YSZ), Pt/YSZ, Ni/scandia-stabilized zirconia, Ni/titania/YSZ. For all electrode types besides those with a continuous titania interlayer a triple phase boundary (TPB) and an area pathway could be separated. Moreover, activation energies as well as hydrogen and water reaction orders were determined for both pathways and compared with previously published data on Ni/YSZ. It was found that when varying the electronically conducting phases on YSZ the activation energy of the TPB path remains virtually the same. However, changing the ion conductor significantly influenced the activation energy, indicating a rate-limiting step on the electrolyte. However, the stark difference in water reaction order of Ni/YSZ and Pt/YSZ electrodes shows that the metal phase is also actively participating in the reaction chain. It is suggested that the electrolyte surface is responsible for the rate-limiting electrochemical redox reaction while the metal interacts with the gas phase molecules and thus supplies the reactants. For samples with a thin mixed conducting titania layer on YSZ, the electrochemical behavior drastically changed, which can be explained by an extension of the reaction zone away from the TPB.

1. Introduction

Solid oxide fuel cells (SOFCs) are a promising technology for the conversion of chemical energy to electrical energy due to their high efficiency compared to Carnot-limited engines, low pollutant emission, and much higher fuel-flexibility than proton exchange membrane fuel cells. In the last 25 years, much research effort has been put into increasing the power density and lifetime of SOFCs by optimization of cathodes and introduction of novel cathode materials [1, 2]. Owing to the related achievements on cathode performance, research dealing with the resistive losses at the anode has again come more into focus, especially for applications employing carbon and sulfur containing fuels. Despite many studies investigating the electrochemical properties of SOFC anodes in general and Ni/yttria stabilized zirconia (YSZ) in particular [3–27], the basic reaction mechanisms at metal/ceramic anodes are still not completely understood.

Fundamental studies dealing with the electrochemistry of Ni/YSZ anodes often utilized micro-structured thin film electrodes, which offer the advantage of a much better defined geometry compared to porous cermet electrodes. With such model electrodes, convoluting factors like gas- or oxide ion diffusion can be avoided [3, 10–12, 14, 15, 17, 18, 27–29]. Moreover, electrodes with well-defined geometry can be used to compare different materials without geometrical uncertainties due to processing parameters. In a previous study, Ni/YSZ electrodes with varying triple phase boundary (TPB) length or surface area were electrochemically characterized in H_2/H_2O atmosphere, leading to the discovery that Ni/YSZ electrodes are not purely TPB active, but also

exhibit a reaction path through the electrode bulk including charge transfer at the Ni/YSZ interface [30]. Moreover, activation energies and hydrogen/water reaction orders could be determined for both reaction pathways. Other metal/YSZ systems in H_2/H_2O are much less investigated and only little comparative data exists [31].

The present study aims at a deeper and more general understanding of the reaction mechanisms on metal/ceramic composite electrodes in hydrogen/water atmosphere by extending the parameter space from geometrical variations to the variation of materials. In particular, the material combinations of Pt/YSZ, Ni/scandia stabilized zirconia (SSZ), and Ni/ titania/YSZ are investigated and compared to the previously studied Ni/YSZ. Impedance spectroscopy measurements were performed on micro-patterned thin-film model electrodes of these material combinations and the measurement temperature as well as the partial pressures of H_2 and H_2O in the atmosphere were systematically varied. This revealed information on the activation energy of the polarization resistance and the reaction orders of the reaction $H_2 + O_O^{\times} \rightleftarrows H_2O + V_O^{\cdot\cdot} + 2e'$ for all material combinations. Based on this comparison, mechanistic conclusions can be drawn.

2. Experimental

All electrodes were prepared on $10 \times 10 \times 0.5\,mm^3$ (111) oriented YSZ single crystals (9.5 mol% Y_2O_3, Crystec, GER). A porous Ni/YSZ counter electrode was applied on the unpolished bottom side of these substrates by consecutively screen printing NiO/YSZ and Ni paste (Heraeus, GER) and subsequently sintering the sample at 1250 °C for 2 h in air. On the polished YSZ top side, the following different types of working electrodes were grown by pulsed laser deposition (PLD) and/or magnetron sputtering:

- Pt/YSZ: 400 nm of Pt (99.95%, Ögussa, AT) was grown on the polished top side of the YSZ crystal by sputter deposition (MED020 Coating system, BAL-TEC, LIE) at 2×10^{-2} mbar Ar with a current of 100 mA. The metal film was then recrystallized at 800 °C in a reducing atmosphere containing 2.5 kPa H_2/0.15 kPa H_2O/balance Ar (denoted H2.5W10 in the following). Micro-structuring of the film was done by photolithography (photoresist: ma-N 1420, developer: ma-D 533S, both: Micro Resist Technology GmbH, GER) and Ar ion etching (3 kV, about 2 mA ion current).
- Ni/SSZ: first, 60 nm of scandia stabilized zirconia (6 mol% Sc_2O_3, Treibacher, AT) were deposited on the top side of the YSZ crystal via PLD at 650 °C substrate temperature in 4×10^{-2} mbar O_2 with a target-to-substrate distance of 6 cm. For the target ablation a KrF excimer laser (Compex Pro 201F KrF Excimer laser, Coherent, USA) with 400 mJ/pulse and 5 Hz pulse frequency was used; the deposition time was 20 min. Then, 1200 nm of Ni (99.99%, Advent RM, UK) were deposited by magnetron sputtering at 8×10^{-3} mbar Ar with a current of 150 mA and the film was recrystallized at 800 °C in H2.5W10 atmosphere. Finally, the Ni film was micro-structured by photolithography (as described above) and chemical etching in aqua regia.
- Ni/TiO_2/YSZ: 30 nm TiO_2 were deposited on the top side of the YSZ crystal by sputtering a Ti target (BAL-TEC) at 7×10^{-3} mbar Ar and equilibrating the obtained layer for 3 h at 800 °C in air. In [32] it is shown that anatase is formed by this procedure. Afterwards, 1200 nm Ni were deposited, recrystallized, and structured as described for Ni/SSZ.

Micro-structuring of the metal films led to samples covered with many working electrodes with nominally constant TPB length of 4.03 mm but varying area as described in [30, 33]. A sketch of the electrode shapes is given in figure 1(a). After film growth and micro-patterning all samples were annealed at 800 °C in H2.5W10 atmosphere for 10^6 s (i.e. ca. 278 h) to stabilize the electrochemical properties. (see [34] for more details). Subsequently, the pattern electrodes were geometrically characterized by optical microscopy. Electrochemical impedance spectroscopy (Alpha-A high performance frequency analyzer with POT/GAL interface, Novocontrol, GER) was performed in a symmetrically heated micro-contact setup (Huber Scientific, AT), which offers the opportunity of contacting four electrodes at once and addressing them subsequently. For details regarding this setup the reader is referred to [35]. Several exemplary impedance spectra are shown in figure 1(b) for Ni/SSZ microelectrodes of different shape and area (but identical TPB length) and for identical shapes but different materials (Pt/YSZ, Ni/SSZ and, for comparison, also Ni/YSZ from [30]). All spectra could be fitted to a simple equivalent circuit (see figure 1) consisting of an electrolyte spreading resistance R_{spread} and a resistor in parallel to a constant phase element. The latter resistor R_{Pol} revealed the polarization resistance of the electrochemical reaction, see also [30]. Spectra for Ni/TiO_2/YSZ including their analysis are described in the corresponding chapter.

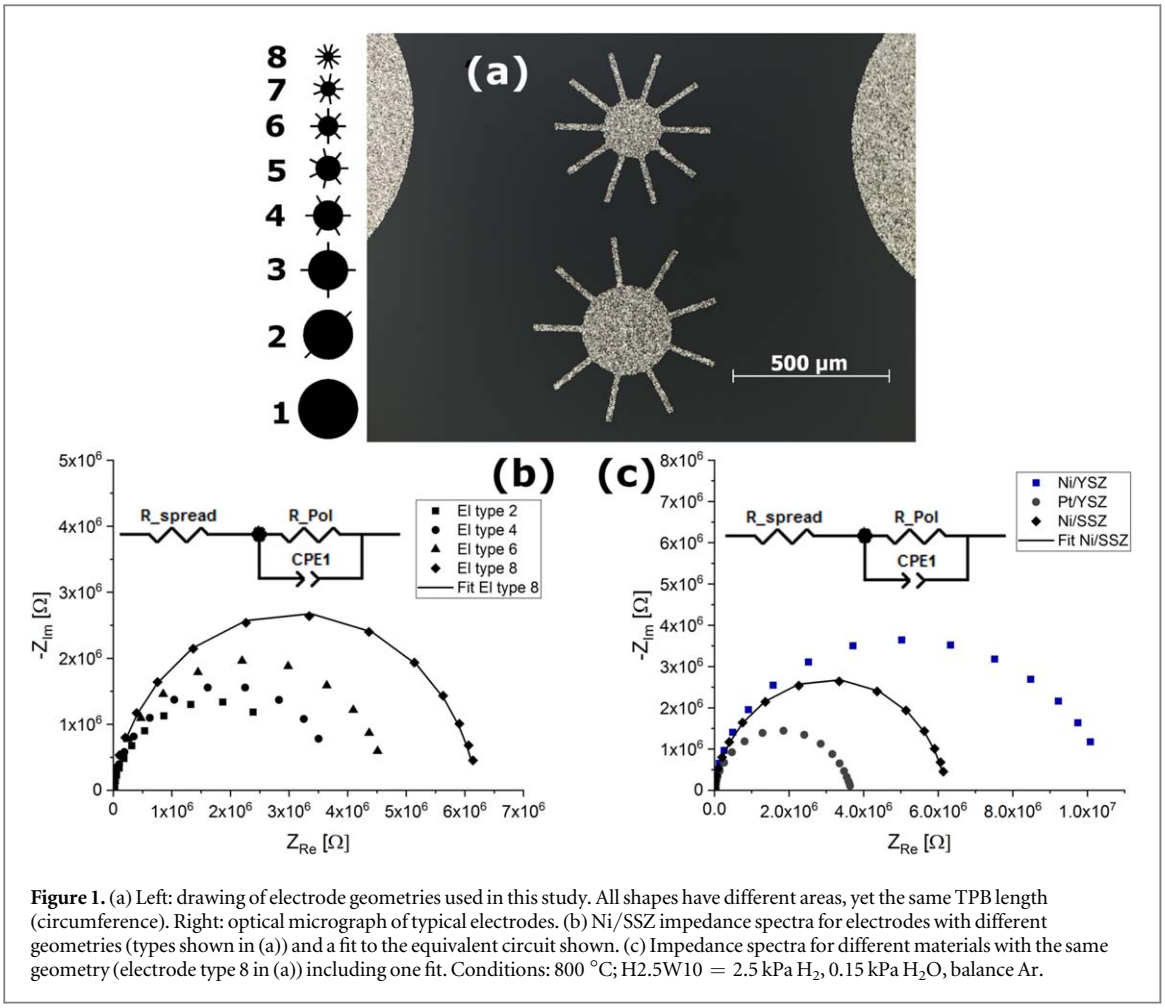

Figure 1. (a) Left: drawing of electrode geometries used in this study. All shapes have different areas, yet the same TPB length (circumference). Right: optical micrograph of typical electrodes. (b) Ni/SSZ impedance spectra for electrodes with different geometries (types shown in (a)) and a fit to the equivalent circuit shown. (c) Impedance spectra for different materials with the same geometry (electrode type 8 in (a)) including one fit. Conditions: 800 °C; H2.5W10 = 2.5 kPa H_2, 0.15 kPa H_2O, balance Ar.

3. Results

3.1. Pt/YSZ

3.1.1. Geometry dependence

Pt electrodes with constant TPB length but varying area were electrochemically characterized by impedance spectroscopy at 800 °C in H2.5W10 atmosphere (2.5 kPa H_2, 0.15 kPa H_2O, balance Ar). The resulting inverse polarization resistances (electrode conductances) are plotted as a function of the electrode area in figure 2(a) (black squares). Similar to the reference material Ni/YSZ (gray triangles, data from [30]), a *y*-axis intercept as well as a linear correlation between conductance and electrode area is found. Therefore, the electrode cannot be purely TPB active, since an increase in electrode area at constant TPB length also increases the activity/conductance of the electrode. In accordance with [30] this geometry dependence of the conductance is interpreted in terms of two distinct parallel reaction pathways for hydrogen oxidation being present for Pt/YSZ electrodes, a 'TPB pathway', represented by the *y*-axis intercept in figure 2(a), and an 'area pathway', which is reflected by the slope in the conductance versus area plot. The respective geometry-normalized conductances for both pathways are summarized in table 1 and further discussed below.

3.1.2. Activation energies

The slopes *k* and intercepts *d* from the conductance-area diagrams at different temperatures (figure 2(b)) can be plotted in an Arrhenius diagram as shown for Pt/YSZ and Ni/YSZ in figure 2(c). The slopes *k* (in S m^{-2}) correspond to the area specific conductance of the area pathway and the intercept *d* (in S) is the inverse resistance of the TPB pathway of the corresponding electrode type with 4.03 mm TPB length. The activation energies are summarized in table 1. The Arrhenius plot shows that for the TPB pathway (intercepts, *d*) the activation energy of Pt/YSZ (2.19 ± 0.08 eV) is very similar to the activation energy in the Ni/YSZ system (1.96 ± 0.07 eV [30]). The area pathway, on the other hand, shows a significantly different activation energy with 1.49 ± 0.01 eV in the Pt/YSZ system compared to 1.04 ± 0.04 eV for Ni/YSZ [30].

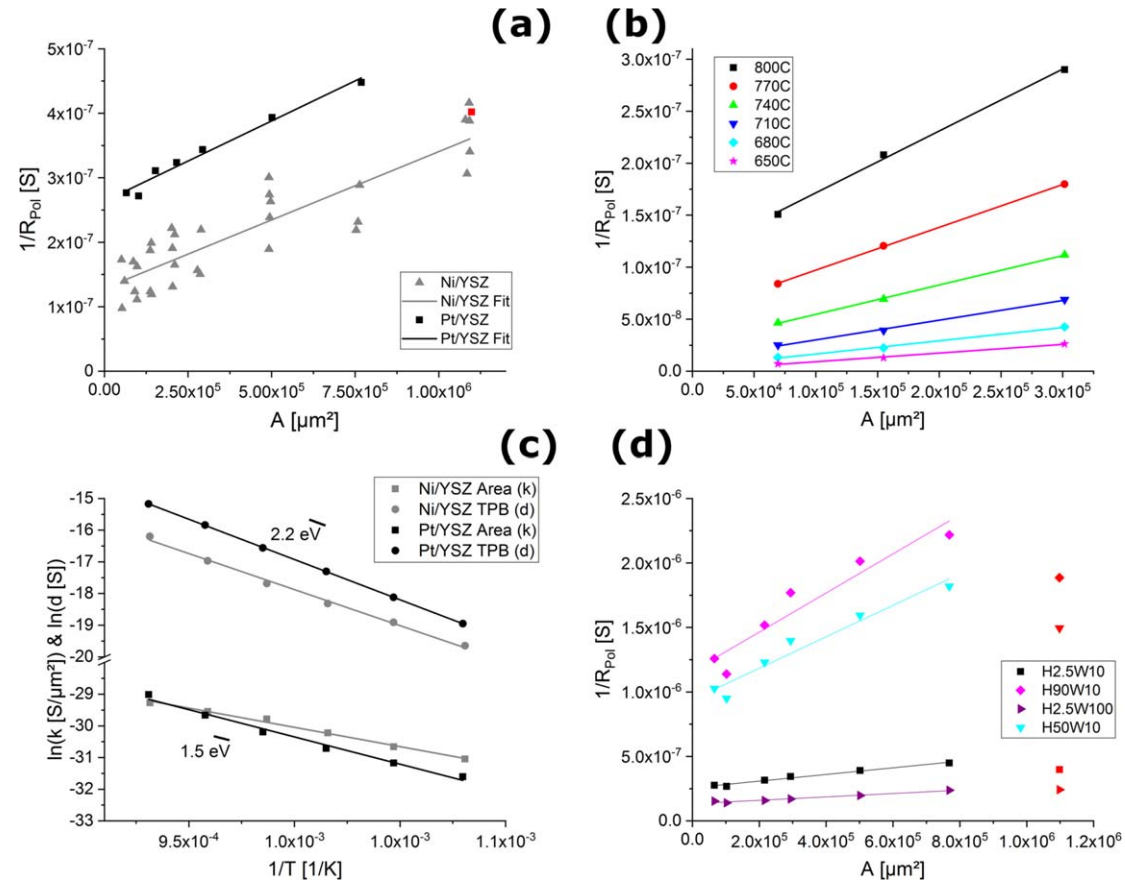

Figure 2. Pt/YSZ data. (a) Electrode conductance($1/R_{Pol}$)-area(A) diagram for Pt/YSZ (black squares, the red symbol shows an outlier) and the reference material Ni/YSZ (gray triangles); conditions: 800 °C, H2.5W10. (b) $1/R_{Pol}$ versus A diagram for Pt/YSZ at different temperatures. (c) Arrhenius diagram of the parameters k (slope in S m^{-2}) and d (intercept in S) from (b), reflecting the inverse polarization resistances of the area- and TPB-pathway of Pt/YSZ; atmosphere: H2.5W10. (d) $1/R_{Pol}$-A diagram at 800 °C for different gas compositions (the red symbols denote outliers); H2.5W10 = 2.5 kPa H_2, 0.15 kPa H_2O, H90W10 = 90 kPa H_2, 0.15 kPa H_2O, H2.5W100 = 2.5 kPa H_2, 1.5 kPa H_2O.

Table 1. Summary of measured geometry related electrodes conductances (LSC = line specific conductance (d/4.03 mm), ASC = area specific conductance (k), both at 800 °C in H2.5W10), activation energies, and hydrogen, water, and oxygen reaction orders (RO) of both pathways obtained in this study and from an expanded data set from [30] (shown as Ni/YSZ reference in the figures). Water reaction orders of Ni/SSZ are not listed as they are not sufficiently reliable.

	TPB pathway					Area pathway				
Material	LSC S m^{-1}	Ea eV	RO H_2	RO H_2O	RO O_2	ASC S m^{-2}	Ea eV	RO H_2	RO H_2O	RO O_2
Ni/YSZ	3.2×10^{-5}	1.96	0.38	0.35	—	0.21	1.04	0.50	0.35	—
Pt/YSZ	6.5×10^{-5}	2.19	0.42	−0.28	−0.19	0.25	1.48	0.50	−0.29	−0.22
Ni/SSZ	4.9×10^{-5}	1.42	0.35	*n.r.*	—	0.16	1.27	0.54	*n.r.*	—
TiO_2/Ni (etched)	1.3×10^{-4}	2.13	0.49	0.32	—	—	—	—	—	—
TiO_2/Ni (unetched)	7.7×10^{-3}	0.48	0.33	−0.16	—	—	—	—	—	—

3.1.3. $H_2/H_2O/O_2$ reaction orders

To obtain partial reaction orders of the electrochemical reaction $H_2 + O_O^x \rightleftharpoons H_2O + V_O^{\cdot\cdot} + 2e'$, electrodes were measured in varying partial pressures of hydrogen and water. When assuming a simple power law, the reaction order may be determined from a double-logarithmic diagram of the inverse polarization resistance of each pathway versus partial pressure according to the equation

$$\log(1/R_{path}) = \zeta_x \log(p_x) + const \quad (1)$$

with ζ_x denoting the partial reaction order and p_x the corresponding partial pressure. When plotting slopes k (area specific conductance of the area pathway) and intercepts d (conductance of the TPB pathway) obtained from the conductance-area diagrams (see figure 2(d)) in such double-logarithmic diagrams, reaction orders of the respective pathways can thus be obtained. The resulting collection of reaction order diagrams for Pt/YSZ is

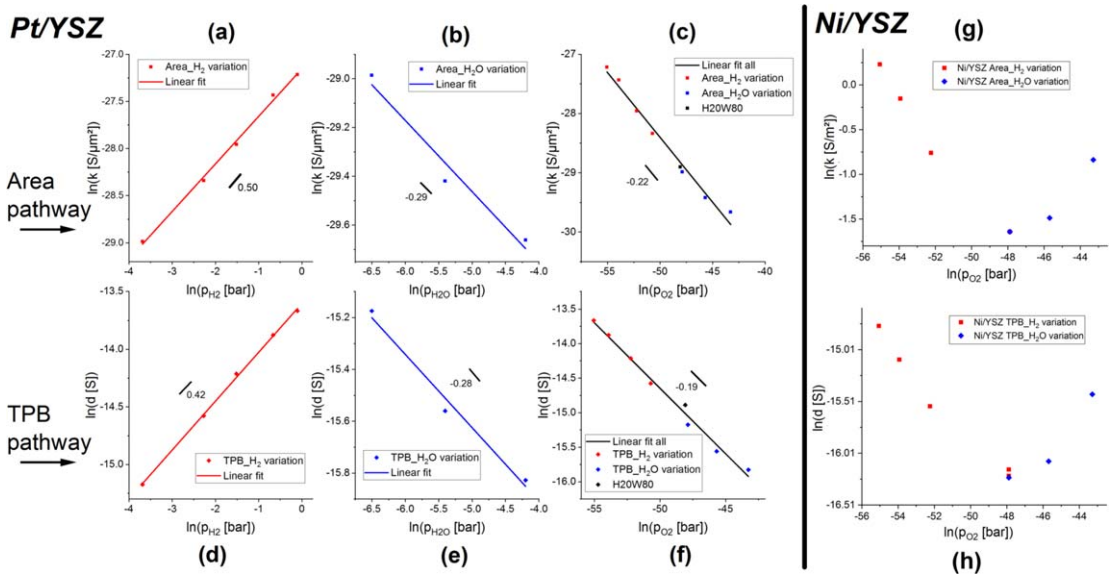

Figure 3. Pt/YSZ reaction order diagrams for H_2 (a), (d), H_2O (b), (e), and O_2 (c), (f) for both the area pathway (a)–(c) and the TPB pathway (d)–(f) at 800 °C. Oxygen reaction order diagrams of Ni/YSZ from [30] are shown in (g) (area pathway) and (h) (TPB pathway) for comparison. Equilibrium oxygen partial pressures are calculated using NIST data [36]. H20W80 = 20 kPa H_2, 1.2 kPa H_2O, balance Ar.

shown in figure 3. The figure shows that reaction order values for hydrogen and water are in the range of $+1/2$ and $-1/4$, respectively, irrespective of the reaction pathway. Moreover, a nominal oxygen partial pressure can be determined from $p_{O_2} = (p_{H_2O}/p_{H_2})^2\ K^{-1}$ (the equilibrium constant K was calculated from thermodynamic data [36]) and for both pathways a simple reaction order is found also for oxygen ($\sim -1/5$). From this result, one may speculate that on Pt/YSZ H_2 and H_2O do not affect the polarization resistance independently. Rather, the influence of the H_2 and H_2O partial pressure on the polarization resistance possibly occurs via the equivalent equilibrium oxygen partial pressure. This is in constrast to Ni/YSZ where even the sign of the water reaction order (+0.35) is different [30]. The calculated reaction orders are summarized in table 1.

3.2. Ni/SSZ

3.2.1. Geometry dependence

Analogously to Pt/YSZ, also Ni/SSZ micro-electrodes were measured at 800 °C in H2.5W10 atmosphere. Exemplary spectra are depicted in figures 1(b) and (c) and show the same shape as for Pt/YSZ and the reference Ni/YSZ. The area dependency of the conductance is given in figure 4(a), together with a linear fit of the data. In accordance with Pt/YSZ and Ni/YSZ [30], again two parallel reaction pathways are found—one scaling with the TPB length, the other one with the electrode area. The absolute values of the area specific conductance of the area pathway and line specific conductance of the TPB pathway are summarized in table 1.

3.2.2. Activation energies

Impedance measurements of the Ni/SSZ electrodes were also conducted at varying temperatures. For each measured temperature, slopes k (area pathway) and intercepts d (TPB pathway) were extracted from conductance-area diagrams and plotted in an Arrhenius diagram, which is depicted in figure 4(c). From that plot activation energies of 1.27 ± 0.11 eV and 1.42 ± 0.07 eV can be extracted for the area and TPB pathway of Ni/SSZ, respectively. It is remarkable that the activation energy of the TPB pathway is more than 0.5 eV lower than for both YSZ-related systems mentioned above (Pt/YSZ, Ni/YSZ). This significantly lower activation energy of Ni/SSZ was also confirmed in a second identical measurement series [34], thus excluding a measurement error or a fit artifact as possible reason for this difference. Rather, this observation points towards an important role of the electrolyte in the TPB pathway—further details are discussed below.

3.2.3. H_2/H_2O reaction orders

Again, reaction orders of both reaction pathways on Ni/SSZ were extracted by determining the slopes k (area pathway) and intercepts d (TPB pathway) in conductance-area diagrams for different gas compositions (see figure 4(d)) and plotting the resulting data set in double logarithmic diagrams against partial pressures, see figure 5. As can be seen in the conductance-area plot (figure 4(d)) some data for the water partial pressure variation scatter significantly (the relative standard deviation of the area pathway activity of H2.5W100 is 340%,

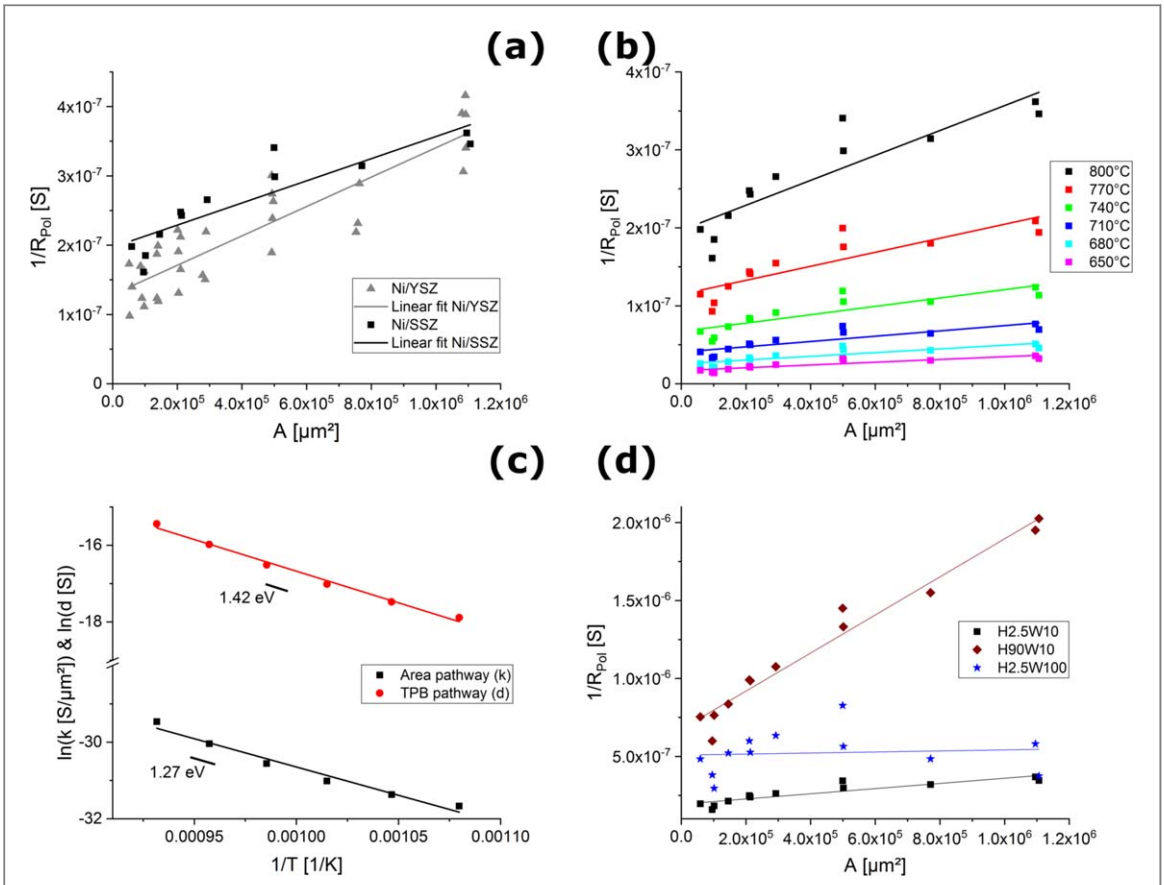

Figure 4. Ni/SSZ data. (a) Electrode conductance-area diagram for Ni/SSZ (black squares) and the reference material Ni/YSZ (gray triangles); conditions: 800 °C, H2.5W10. (b) $1/R_{Pol}$-A diagram for Ni/SSZ at different temperatures. (c) Arrhenius diagram of the two fit parameters k (in S m^{-2}) and d (in S) representing the area- and TPB-pathway of Ni/SSZ; atmosphere: H2.5W10. (d) $1/R_{Pol}$-A diagram at 800 °C for different gas compositions; H2.5W10 = 2.5 kPa H_2, 0.15 kPa H_2O, H90W10 = 90 kPa H_2, 0.15 kPa H_2O, H2.5W100 = 2.5 kPa H_2, 1.5 kPa H_2O.

while for H2.5W10 it is only 15%), which results in substantial uncertainty of the water reaction orders. The reliably obtained H_2 reaction orders were extracted according to equation (1) and are summarized in table 1.

3.3. Ni/TiO_2/YSZ

3.3.1. Impedance spectrum

The impedance spectrum of a Ni/TiO_2/YSZ sample with continuous TiO_2 interlayer is shown in figure 6(a). It can be seen that the Nyquist plot clearly shows two arcs. These spectra were fitted to the equivalent circuit shown in the inset of the figure in the frequency range of 100 Hz–5 mHz. Additional electrode features at higher frequencies are neglected in this fit. The total polarization resistance was calculated by summing all resistance values in the equivalent circuit ($R_{Pol} = R1 + R2 + R3$); please note that for the sake of simplicity the small contribution of the electrolyte was not separated in this case. The obtained polarization resistance is about two orders of magnitude lower than for all other electrode types. Reasons for this behavior are discussed below.

Removing the uncovered TiO_2 layer by Ar ion bombardment completely changed the electrochemical behavior, yielding again an impedance response very similar to Ni/YSZ, Ni/SSZ or Pt/YSZ—i.e. an electrode feature consisting of one slightly asymmetric semicircle; compare figure 5(b) with figures 1(b) and (c). Also, the same fitting approach could be successfully applied as for the metal/zirconia based electrodes.

3.3.2. Geometry dependence

Again, electrodes with varying area but constant TPB length were measured at 800 °C in H2.5W10 atmosphere. The inverse polarization resistances obtained for continuous TiO_2 layer samples are compared with Ni/YSZ in figure 7(a). From this plot it is obvious that the electrode conductances were much higher than those of Ni/YSZ electrodes, which may already indicate a completely different reaction mechanism on that type of samples.

Removal of the titania interlayer not being covered by Ni changes the polarization resistance drastically. A plot of the electrode conductance $1/R_{Pol}$ of such an etched samples versus the electrode area is shown in figure 7(b). It can be seen that the conductances of the etched samples are still somewhat higher than for Ni/YSZ electrodes, but at least in the same order of magnitude.

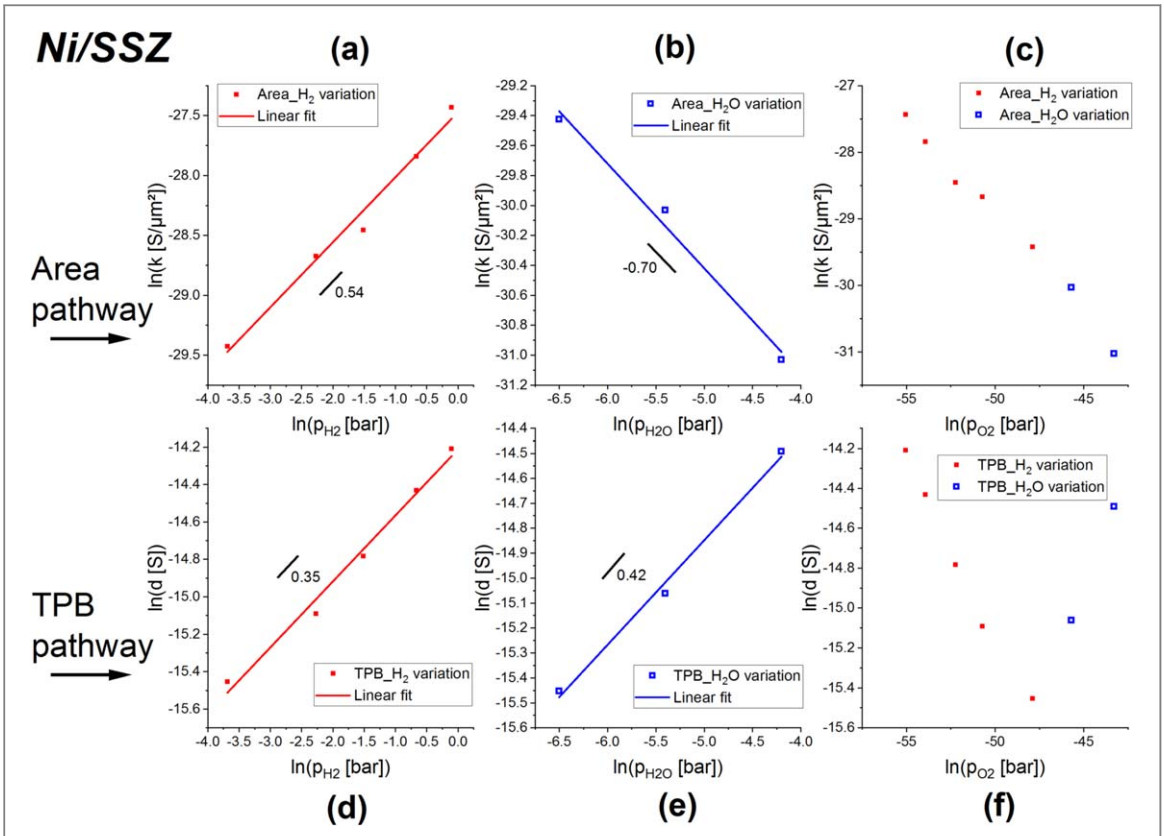

Figure 5. Ni/SSZ reaction order diagrams at 800 °C for H_2 (a), (d), H_2O (b), (d), and O_2 (c), (f) for both the area pathway (a)–(c) and the TPB pathway (d)–(f). Equilibrium oxygen partial pressures are calculated using NIST data [36]. The water reaction orders have to be considered with caution (see scattering data in figure 4(d))—the corresponding points are indicated by open symbols.

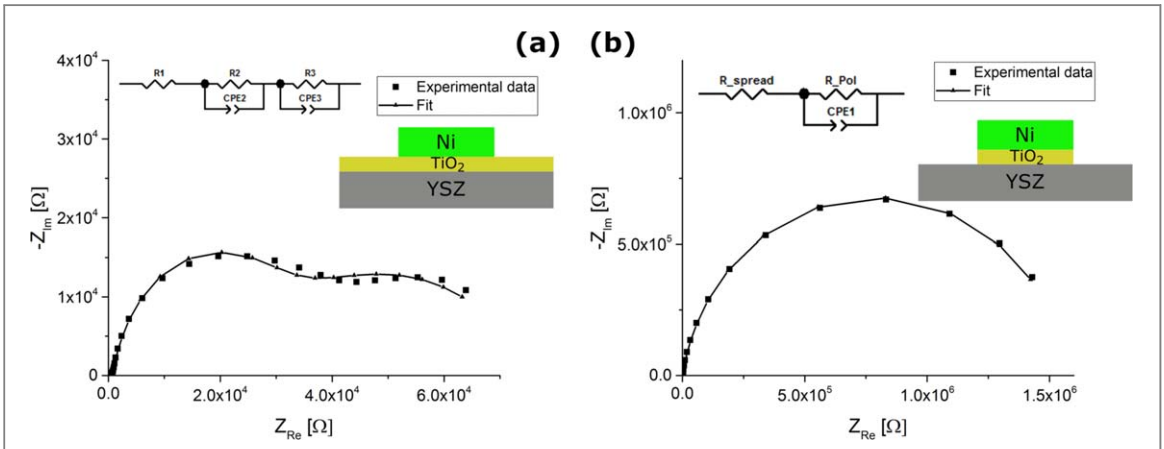

Figure 6. Nyquist plots of $Ni/TiO_2/YSZ$ electrodes measured at 800 °C in H2.5W10 with equivalent circuits for fitting. (a) Spectrum obtained for a complete titania layer and (b) with uncovered titania being etched away. For the latter, the same fitting strategy as for Ni/YSZ can be employed.

Analysis of the electrode conductance values does not confirm statistical significance for the existence of an area pathway. In both cases the slope does not deviate from zero with $p < 0.05$, therefore the average conductance of all measured electrodes was summarized as TPB pathway activity in table 1.

3.3.3. Activation energy

Measurements on etched and non-etched $Ni/TiO_2/YSZ$ samples were also conducted at different temperatures. Since no area pathway could be confirmed, only activation energies of the polarization resistance of individual electrodes were derived. The Arrhenius diagram comparing results on both etched and non-etched samples is depicted in figure 7(c). This plot shows that after removing the uncovered TiO_2 layer the electrodes exhibit an activation energy of 2.10 ± 0.14 eV, which is close to that of the reference Ni/YSZ TPB activation energy

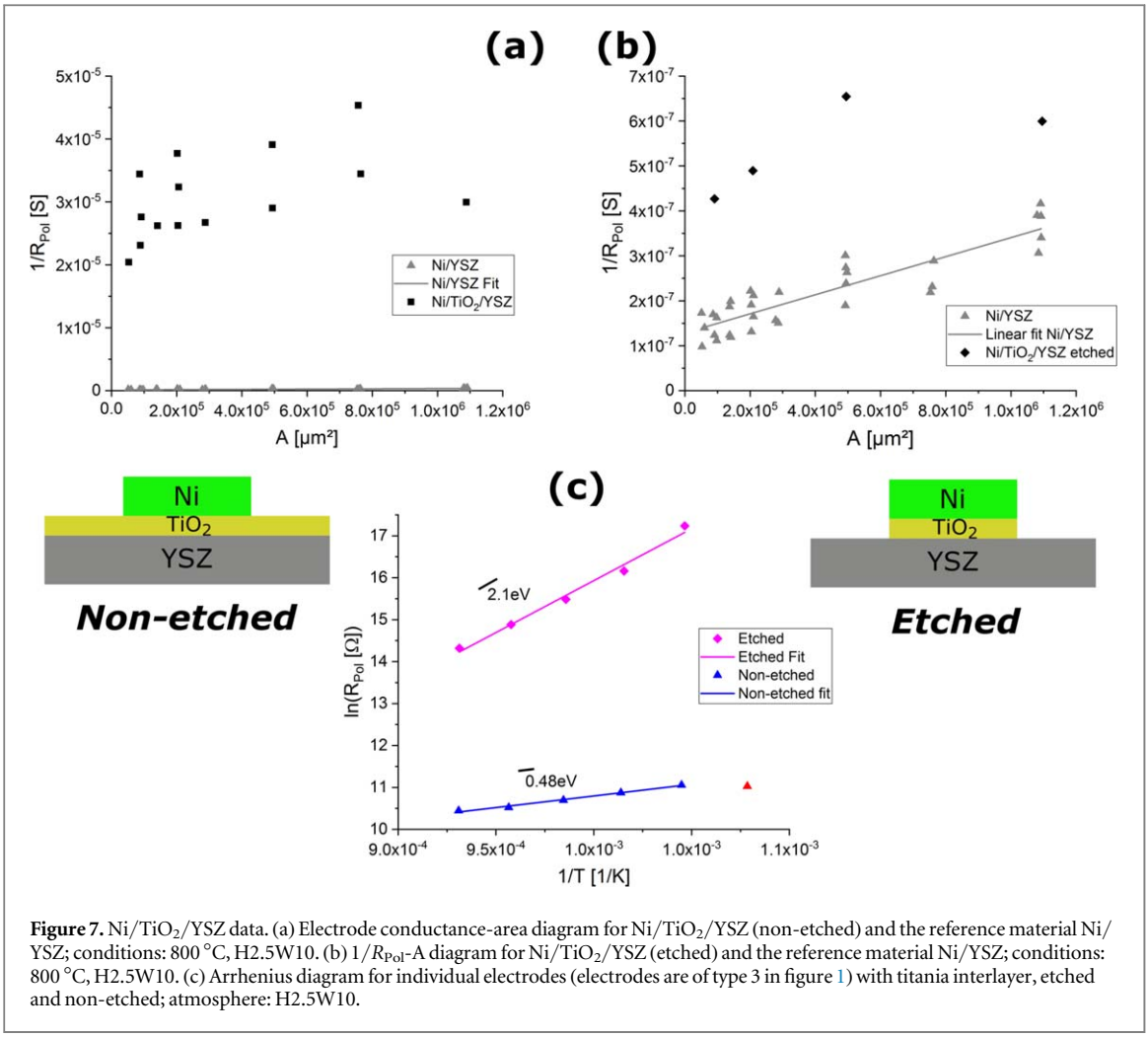

Figure 7. $Ni/TiO_2/YSZ$ data. (a) Electrode conductance-area diagram for $Ni/TiO_2/YSZ$ (non-etched) and the reference material Ni/YSZ; conditions: 800 °C, H2.5W10. (b) $1/R_{Pol}$-A diagram for $Ni/TiO_2/YSZ$ (etched) and the reference material Ni/YSZ; conditions: 800 °C, H2.5W10. (c) Arrhenius diagram for individual electrodes (electrodes are of type 3 in figure 1) with titania interlayer, etched and non-etched; atmosphere: H2.5W10.

(1.96 ± 0.07 eV). The non-etched electrode, on the other hand, is activated by only 0.48 ± 0.03 eV. Such a severe difference of activation energies strongly suggests a completely different reaction mechanism—see discussion below.

3.3.4. H_2/H_2O reaction orders

Analogously to the previous sections, water and hydrogen reaction orders were determined for the entire polarization resistance of etched and non-etched $Ni/TiO_2/YSZ$ samples. The corresponding reaction order diagrams are shown in figure 8 and the extracted reaction orders are summarized in table 1. Differences are particularly pronounced with respect to H_2O.

4. Discussion

The results of non-etched $Ni/TiO_2/YSZ$ samples differ strongly from all other experiments. They show a surprisingly high electrode conductance and a very low activation energy (0.48 eV). However, the situation changes when removing the parts of the titania layer not covered by Ni. The conductance sharply decreases and approaches the values of pure Ni/YSZ. This very different behavior of non-etched films can be explained by an expansion of the reaction zone along the free titania surface and is discussed in more detail below. All electrodes with YSZ being part of the TPB, i.e. Ni/YSZ, Pt/YSZ, and etched $Ni/TiO_2/YSZ$, exhibit very similar activations energies in the range of 2 eV. The TPB pathway of Ni on scandia stabilized zirconia, on the other hand, shows a significantly different activation energy compared to the YSZ-based TPBs. This indicates that the activation energy depends primarily on the electrolyte phase and suggests that the rate limiting step is located on/in the electrolyte rather than on the metal. Possibly, the rate limiting step on/in the electrolyte includes an electron-related process such as charge transfer to a surface species and/or electron transport in the electrolyte.

This importance of the electrolyte, however, does not exclude any mechanistic role of the metal phase on YSZ. Information on the role of the metal is gained from the reaction orders of the TPB pathway in different

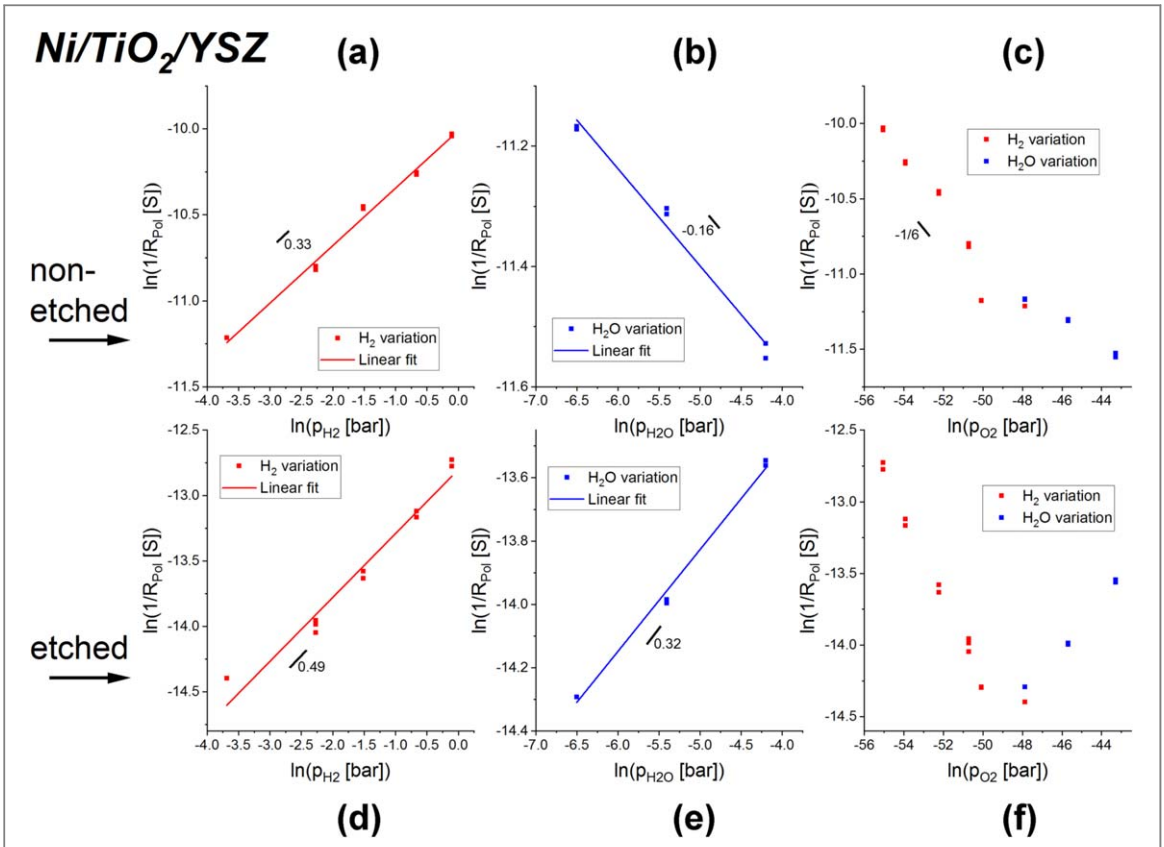

Figure 8. Reaction order diagrams of $Ni/TiO_2/YSZ$ electrodes at 800 °C for H_2 (a), (d), H_2O (b), (d), and O_2 (c), (f) for both the un-etched (a)–(c) and etched (d)–(f) samples. Equilibrium oxygen partial pressures are calculated using NIST data [36].

systems. The hydrogen reaction order of the TPB pathway varies only slightly for Ni/YSZ, Ni/SSZ, $Ni/TiO_2/YSZ$ and Pt/YSZ electrodes (between 0.35 and 0.49), but the water reaction order differs significantly —partly even with different algebraic signs. From these differences we conclude that the metal phase does not only act as a current collector but actively takes part in the reaction chain of the TPB path, most probably via interaction with the gas phase, i.e. adsorption/desorption and/or dissociation. This hypothesis is further supported by the results found for the area pathway.

The available activation energies of the area pathway depend on the metal phase, which is hardly surprising, as all physically meaningful reaction mechanisms for this pathway include a role of the metal [30]). The hydrogen reaction orders of the area pathway are the same for Pt/YSZ and Ni/YSZ. However, strongly different H_2O reaction orders are found, partly with different signs. On the other hand, a close similarity exists for the measured reaction orders of TPB and area pathway of each individual system, i.e. for Ni/YSZ and for Pt/YSZ. Particularly, the water reaction order of TPB and area pathways is virtually identical for a given metal (Ni or Pt). This indicates that the water related part of the TPB and area pathway is probably the same. We therefore suggest that for both pathways the interaction with the gas phase goes via the metal. Hence, the TPB activity of metal/ceramic electrodes seems to rely on a kind of job sharing: the main electrochemical reaction takes place on the electrolyte and the metal is responsible for the supply (or removal) of adsorbed gas species. This adsorbate supply/removal seems to work even if a thin TiO_2 layer is still between Ni and YSZ, see sketch in figure 7.

Finally, the very different behavior of non-etched $Ni/TiO_2/YSZ$ electrodes is discussed in more detail. We suppose that TiO_2 acts as a mixed ionic and electronic conducting electrode under the present experimental conditions. Accordingly, hydrogen is oxidized on larger parts of the TiO_2 surface and oxide ions move across the titania layer, while electrons move in-plane and are collected by the Ni. The main conductance increase of the non-etched $Ni/TiO_2/YSZ$ samples is thus caused by the much larger active area for the electrochemical reaction due to in-plane electron conduction in TiO_2. A very similar situation can be found for ceria based mixed conducting anodes [37, 38]. The rate-limiting process is probably a combination of lateral transport of electrons and electrochemical reaction at the surface of mixed conducting TiO_2. The interpretation of lateral electron transport in titania interlayers being relevant for the polarization resistance of non-etched $Ni/TiO_2/YSZ$ samples is further supported by the reaction orders. While no simple oxygen reaction order can be found for the etched $Ni/TiO_2/YSZ$, non-etched electrodes show a continuous increase of the conductance with decreasing p_{O_2}, see figure 8. From the defect chemical model of undoped TiO_2 [39] an oxygen reaction order of $-1/6$ would

be expected for the electronic conductivity of the titania interlayer, which is rather close to the value observed here.

5. Conclusion

In this study the electro-catalytic properties of micro-structured thin film model electrodes were investigated for the metal/electrolyte combinations Ni/YSZ, Pt/YSZ, Ni/SSZ, Ni/TiO_2/YSZ. By variation of the electrode area while keeping the TPB length constant, an area and a TPB related reaction pathway could be separated for electrodes without TiO_2 interlayer. By variation of temperature as well as hydrogen and water partial pressure, activation energies and reaction orders were determined for both pathways. The resulting data set was compared with previously published data on Ni/YSZ. The comparison of activation energies showed that for all samples with uncovered YSZ electrolyte (i.e. Ni/YSZ, Pt/YSZ, and etched Ni/TiO_2/YSZ) the activation energies were very similar around 2 eV. For Ni/SSZ only 1.4 eV was found. This behavior suggests that the rate-limiting step of the TPB pathway is located on the electrolyte. However, the electronically conducting phase is not an inert current collector, since the metal significantly influences the water reaction order (with even different algebraic sign on Ni/YSZ and Pt/YSZ). Therefore, the metal is suggested to be relevant for the adsorption/desorption of species and their transport to/from the reaction zone on the electrolyte. Deposition of a thin TiO_2 layer onto the YSZ electrolyte before applying the Ni electrodes caused an increase of the electrode activity by about two orders of magnitude. This can be explained by the mixed conducting properties of the titania film at the given experimental conditions, which leads to an extension of the electrochemically active region along the free titania surface.

Acknowledgments

The financial support by the Austrian Federal Ministry of Science, Research and Economy and the National Foundation for Research, Technology and Development is gratefully acknowledged. Huber Scientific (https://sofc.at/) is acknowledged for supporting the development of the micro-contact test station used in this study. The authors also acknowledge the TU Wien University Library for financial support through its Open Access Funding Program.

ORCID iDs

A K Opitz https://orcid.org/0000-0002-2567-1885

References

[1] Adler S B 2004 Factors governing oxygen reduction in solid oxide fuel cell cathodes *Chem. Rev.* **104** 4791–844
[2] Blum L, de Haart L G J, Malzbender J, Menzler N H, Remmel J and Steinberger-Wilckens R 2013 Recent results in Jülich solid oxide fuel cell technology development *J. Power Sources* **241** 477–85
[3] Bessler W G, Vogler M, Stormer H, Gerthsen D, Utz A, Weber A and Ivers-Tiffee E 2010 Model anodes and anode models for understanding the mechanism of hydrogen oxidation in solid oxide fuel cells *Phys. Chem. Chem. Phys.* **12** 13888–903
[4] Gong M, Liu X, Trembly J and Johnson C 2007 Sulfur-tolerant anode materials for solid oxide fuel cell application *J. Power Sources* **168** 289–98
[5] Khan M S, Lee S-B, Song R-H, Lee J-W, Lim T-H and Park S-J 2016 Fundamental mechanisms involved in the degradation of nickel–yttria stabilized zirconia (Ni–YSZ) anode during solid oxide fuel cells operation: a review *Ceram. Int.* **42** 35–48
[6] Liu M, Lynch M E, Blinn K, Alamgir F M and Choi Y 2011 Rational SOFC material design: new advances and tools *Mater. Today* **14** 534–46
[7] Mahato N, Banerjee A, Gupta A, Omar S and Balani K 2015 Progress in material selection for solid oxide fuel cell technology: a review *Prog. Mater Sci.* **72** 141–337
[8] Sarantaridis D and Atkinson A 2007 Redox cycling of ni-based solid oxide fuel cell anodes: a review *Fuel Cells* **7** 246–58
[9] Shri Prakash B, Senthil Kumar S and Aruna S T 2014 Properties and development of Ni/YSZ as an anode material in solid oxide fuel cell: a review *Renew. Sustain. Energy Rev.* **36** 149–79
[10] Bieberle A and Gauckler L J 2000 Reaction mechanism of Ni pattern anodes for solid oxide fuel cells *Solid State Ion.* **135** 337–45
[11] Bieberle A, Meier L P and Gauckler L J 2001 The electrochemistry of Ni pattern anodes used as solid oxide fuel cell model electrodes *J. Electrochem. Soc.* **148** A646–56
[12] Ehn A, Høgh J, Graczyk M, Norrman K, Montelius L, Linne M and Mogensen M 2010 Electrochemical investigation of nickel pattern electrodes in H_2/H_2O and CO/CO_2 atmospheres *J. Electrochem. Soc.* **157** B1588–96
[13] Jensen K V, Wallenberg R, Chorkendorff I and Mogensen M 2003 Effect of impurities on structural and electrochemical properties of the Ni–YSZ interface *Solid State Ion.* **160** 27–37
[14] Li W, Shi Y, Luo Y, Wang Y and Cai N 2015 Carbon deposition on patterned nickel/yttria stabilized zirconia electrodes for solid oxide fuel cell/solid oxide electrolysis cell modes *J. Power Sources* **276** 26–31
[15] Sukeshini A M, Habibzadeh B, Becker B P, Stoltz C A, Eichhorn B W and Jackson G S 2006 Electrochemical oxidation of H_2, CO, and CO/H_2 mixtures on pattERned Ni anodes on YSZ electrolytes *J. Electrochem. Soc.* **153** A705–15

[16] Utz A, Hansen K V, Norrman K, Ivers-Tiffée E and Mogensen M 2011 Impurity features in Ni-YSZ-H_2-H_2O electrodes *Solid State Ion.* **183** 60–70
[17] Utz A, Störmer H, Leonide A, Weber A and Ivers-Tiffée E 2010 Degradation and relaxation effects of Ni patterned anodes in H_2–H_2O atmosphere *J. Electrochem. Soc.* **157** B920–30
[18] Yao W and Croiset E 2015 Stability and electrochemical performance of Ni/YSZ pattern anodes in H_2/H_2O atmosphere *Can. J. Chem. Eng.* **93** 2157–67
[19] Hauch A, Jensen S H, Bilde-Sørensen J B and Mogensen M 2007 Silica segregation in the Ni/YSZ electrode *J. Electrochem. Soc.* **154** A619–26
[20] Jiang S P and Ramprakash Y 1999 H_2 oxidation on Ni/Y-TZP cermet electrodes—a comparison of electrode behaviour by GCI and EIS techniques *Solid State Ion.* **122** 211–22
[21] Koide H, Someya Y, Yoshida T and Maruyama T 2000 Properties of Ni/YSZ cermet as anode for SOFC *Solid State Ion.* **132** 253–60
[22] Pan W, Chen K, Ai N, Lü Z and Jiang S P 2016 Mechanism and Kinetics of Ni–Y_2O_3–ZrO_2 hydrogen electrode for water electrolysis reactions in solid oxide electrolysis cells *J. Electrochem. Soc.* **163** F106–14
[23] Rojek-Wöckner V A, Opitz A K, Brandner M, Mathé J and Bram M 2016 A novel Ni/ceria-based anode for metal-supported solid oxide fuel cells *J. Power Sources* **328** 65–74
[24] Wilson J R, Kobsiriphat W, Mendoza R, Chen H-Y, Hiller J M, Miller D J, Thornton K, Voorhees P W, Adler S B and Barnett S A 2006 Three-dimensional reconstruction of a solid-oxide fuel-cell anode *Nat. Mater.* **5** 541–4
[25] Lin Y, Zhan Z, Liu J and Barnett S A 2005 Direct operation of solid oxide fuel cells with methane fuel *Solid State Ion.* **176** 1827–35
[26] Yang L, Choi Y, Qin W, Chen H, Blinn K, Liu M, Liu P, Bai J, Tyson T A and Liu M 2011 Promotion of water-mediated carbon removal by nanostructured barium oxide/nickel interfaces in solid oxide fuel cells *Nat. Commun.* **2** 357
[27] Mizusaki J *et al* 1994 Preparation of nickel pattern electrodes on YSZ and their electrochemical properties in H_2–H_2O atmospheres *J. Electrochem. Soc.* **141** 2129–34
[28] Utz A, Störmer H, Leonide A, Weber A and Ivers-Tiffee E 2009 Degradation effects of Ni patterned anodes in H_2/H_2O atmosphere *ECS Trans.* **25** 2013–21
[29] Yao W and Croiset E 2013 Ni/YSZ pattern anodes fabrication and their microstructure and electrochemical behavior changes in H_2–H_2O environments *J. Power Sources* **226** 162–72
[30] Doppler M C, Fleig J, Bram M and Opitz A K 2018 Hydrogen oxidation mechanisms on Ni/yttria stabilized zirconia anodes: Separation of reaction pathways by geometry variation of pattern electrodes *J. Power Sources* **380** 46–54
[31] Kek D, Mogensen M and Pejovnik S 2001 A study of metal (Ni, Pt, Au)/Yttria-stabilized zirconia interface in hydrogen atmosphere at elevated temperature *J. Electrochem. Soc.* **148** A878–86
[32] Walch G 2016 Effects of light on mixed conducting electrodes in high-temperature solid oxide electrochemical cells *PhD Thesis* Faculty of Technical Chemistry, TU Wien
[33] Doppler M C, Fleig J, Bram M and Opitz A K 2016 The capacitance of nickel pattern electrodes on zirconia electrolyte *J. Electrochem. Soc.* **163** H1019–25
[34] Doppler M C 2018 On the Electrochemistry of YSZ/Ni and Related Model Electrodes *PhD Thesis* Faculty of Technical Chemistry, TU Wien
[35] Huber T M, Opitz A K and Fleig J 2015 Oxygen reduction via grain boundary transport in thin film platinum electrodes on yttria stabilized zirconia *Solid State Ion.* **273** 8–12
[36] NIST Chemistry WebBook NIST Standard Reference Database Number 69 (https://webbook.nist.gov/chemistry/)
[37] Chueh W C, Hao Y, Jung W and Haile S M 2011 High electrochemical activity of the oxide phase in model ceria–Pt and ceria–Ni composite anodes *Nat. Mater.* **11** 155
[38] Nenning A, Navickas E, Velicsanyi P, Opitz A K, Hutter H and Fleig J 2015 Mapping electrochemically driven gas exchange of mixed conducting $SrTi_{0.7}Fe_{0.3}O_{3-\delta}$ and $Ce_{0.8}Gd_{0.2}O_{1.9}$ thin films by 18O tracer incorporation under reducing atmosphere *Solid State Ion.* **273** 25–9
[39] Nowotny J, Alim M A, Bak T, Idris M A, Ionescu M, Prince K, Sahdan M Z, Sopian K, Teridi M A M and Sigmund W 2015 Defect chemistry and defect engineering of TiO_2-based semiconductors for solar energy conversion *Chem. Soc. Rev.* **44** 8424–42